LOW AND INTERMEDIATE BETA CAVITY DESIGN – A TUTORIAL*

J. R. Delayen, Thomas Jefferson National Accelerator Facility, Newport News, VA 23606, USA

Abstract

The design of low-velocity superconducting structures has been an active area of the superconducting rf (srf) technology for more than 3 decades. More recently, with the growing interest in medium-energy ion and proton accelerators, a sustained world-wide effort has been directed toward the development of the superconducting structures for the intermediate velocity region. In this tutorial we address the design issues that are specific to low- and medium-velocity superconducting cavities. Simple electrostatic and electrodynamic models based on transmission lines are presented, and scaling laws are derived.

INTRODUCTION

Until slightly more than a decade ago the field of superconducting accelerating structures was clearly separated into two distinct velocity regions, each with its own community. The low-velocity structures, designed for the acceleration of protons but mostly for heavy ions, extended to $\beta = v/c \sim 0.2$; these were usually based on resonant transmission lines and will be referred to as TEM structures. The high-velocity structures were used almost exclusively for the acceleration of electrons or positrons and were restricted to $\beta \sim 1$; these were made of a series of coupled cells operating in the TM_{010} mode and will be referred to as TM structures. Since the late 80's there has been a growing interest in higher energy proton accelerators, mostly for spallation sources, and TEM structures have been designed for higher and higher velocities, while TM structures have been designed for lower and lower velocities, until the two have finally overlapped in the $\beta \sim 0.5 - 0.6$ region. An overview and comparison of their basic electromagnetic properties in this overlap region can be found in [1].

Because of the continuous velocity coverage that now exists, the meaning of low-, medium-, and high-velocity structures is somewhat ill-defined and often variable. For the purpose of this paper we will assume that low velocity applies to $\beta \lesssim 0.2$, medium velocity to $0.2 \lesssim \beta \lesssim 0.7$ and high velocity to $\beta \gtrsim 0.7$. With few exceptions, the low-velocity structures are of the TEM class, while the medium-velocity ones are both of the TEM and the TM class.

TM-class structures used in the medium-velocity region are essentially similar to the ones used at high velocity, but with their longitudinal dimensions scaled by β, and the design issues are almost identical. Reviews of the design process of TM cavities (also often called elliptical) can be found in [2, 3], and in this paper we will concentrate on the design issues of low and medium-β TEM structures.

Low velocity means that the velocity of the particle will change as it is accelerated. The lower its velocity, the faster it will change, and the narrower the velocity range of a particular accelerating structures. This implies that the smaller the β of a cavity, the smaller the number of cavities of that β in an accelerator. On the other hand, failure of a low-β cavity to achieve its design gradient may mean that the particle will not be captured by the following section. As a consequence of their small number and importance in achieving design gradient, low-β cavities need to be designed conservatively. As the β is increased they can be designed more aggressively with the expectation of achieving the design gradient on average.

Unlike axially-symmetric TM structures, TEM resonators are essentially 3-dimensional geometries. Several 3D electromagnetic design software packages are available and are capable of calculating frequencies accurately. They can also provide surface electric and magnetic fields but, in this case, the results must be interpreted with caution as they can be sensitive to mesh size and geometry used.

The design of a low-β structure involves several tradeoffs. One is the number of cells. The larger the number of cells the higher the voltage gain, but the narrower the velocity acceptance, and, as a consequence, the larger the number of types of cavities that will need to be designed. The choice of frequency is also important as it affects size, voltage gain, rf losses, microphonics level, rf control, acceptance, beam quality and losses. A detailed discussion of all these issues is beyond the scope of this tutorial and we will concentrate of the electromagnetic design of a structure once the frequency and β have been chosen.

ENERGY GAIN, TRANSIT TIME FACTOR, VELOCITY ACCEPTANCE

The energy gain acquired by a particle traversing an accelerating structure is simply the work done on the particle by the electromagnetic field

$$\Delta W = q \int_{-\infty}^{+\infty} E(z) \cos(\omega t + \phi)\, dz\,, \qquad (1)$$

where q is the charge of the particle, $E(z)$ is the profile of the longitudinal electric field, ω is the angular frequency of the electromagnetic field, and ϕ is the phase of the field when the particle reaches the reference position. The motion of the particle through the cavity is reflected in the relationship between position z and time t. In most cases the field profile is symmetrical and the

* Work supported by the U.S. Department of Energy under contracts DE-AC05-84-ER40150 and DE-AC05-00-OR22725.
# delayen@jlab.org

center of the cavity is chosen as the reference position $z = 0$ and we assume that the particle reaches $z = 0$ at $t = 0$. In Eq. (1) we assumed that the field profile was even with respect to the center of the cavity (odd number of cells or accelerating gaps). In the case of an odd field profile (even number of cells or accelerating gaps) $\cos(\omega t + \phi)$ is replaced by $\sin(\omega t + \phi)$ and all the following results will apply to both cases.

Under the assumption that the energy gain is sufficiently small that the velocity of the particle does not change in the cavity, the energy gain reduces to

$$\Delta W = q \cos\phi \; \Delta W_0 \; T(\beta), \tag{2}$$

where

$$\Delta W_0 = \Theta \int_{-\infty}^{+\infty} |E(z)| \, dz,$$

$$\Theta = \frac{\underset{\beta}{\mathrm{Max}} \int_{-\infty}^{+\infty} E(z) \cos\left(\frac{\omega z}{\beta c}\right) dz}{\int_{-\infty}^{+\infty} |E(z)| \, dz}, \tag{3}$$

$$T(\beta) = \frac{\int_{-\infty}^{+\infty} E(z) \cos\left(\frac{\omega z}{\beta c}\right) dz}{\mathrm{Max} \int_{-\infty}^{+\infty} E(z) \cos\left(\frac{\omega z}{\beta c}\right) dz}.$$

ΔW_0 is the energy gain acquired by a particle of unit charge, and of optimal phase $(\phi = 0)$ and velocity for that cavity; and it can be used to represent the magnitude of the electromagnetic field. Θ is the reduction of the energy gain associated with the time dependence of the field; this quantity is often called, particularly with reference to room temperature structures, the transit time factor. $T(\beta)$ is an additional reduction of the energy gain for particles whose velocity is different from the optimal velocity associated with that cavity. Unfortunately $T(\beta)$ has also often been called, in particular with reference to superconducting structures, the transit time factor; in order to eliminate confusion we will call $T(\beta)$ the velocity acceptance of the resonator. Note that, with the definitions used in Eq. (3) we always have $\Theta < 1$ and $T(\beta) \le T(\beta_0) = 1$, where β_0 is the value of β for which $\int_{-\infty}^{+\infty} E(z) \cos\left(\frac{\omega z}{\beta c}\right) dz$ reaches its maximum value.

Transit-time factors and velocity acceptances can be calculated for field profiles representative of those that can be found in actual cavities. Such field profiles for 1- and 2-loading elements (respectively 2- and 3-gap) TEM structures are shown in Fig 1. The parameter α is used to represent the amount of cavity beam line that is actually filled by the electric field. In TEM structures the cell-to-cell coupling is very large so, in order to obtain a flat field profile, the end cells (side gaps) are actually half-cells so $\int |E(z)| \, dz$ in an end-cell is half what it is in the center cells.

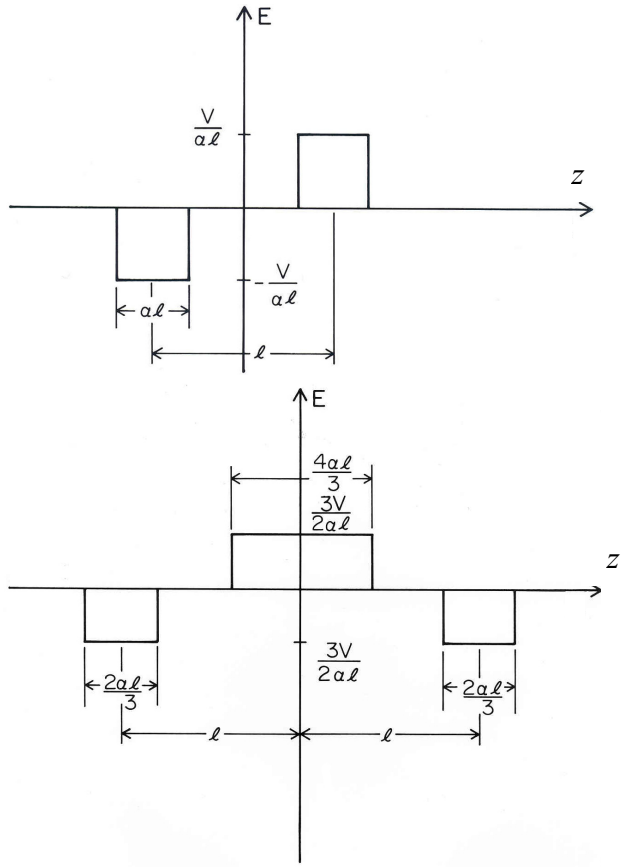

Figure 1: Field profile for 2-gap (a) and 3-gap (b) TEM structures. V is the voltage generated by the transmission line and α is the filling parameter.

Figure 2 shows the transit-time factor Θ for 2- and 3-gap structures. In essence it is the reduction in voltage gain acquired by the optimal particle from the voltage generated in the resonant line.

The velocity acceptance $T(\beta)$ can be calculated for the same field profiles. For a 2-gap structure it is

$$T(\beta) = \frac{\beta}{\beta_0} \frac{\sin\left(\frac{\pi\alpha}{2x_0}\frac{\beta_0}{\beta}\right)\sin\left(\frac{\pi}{2x_0}\frac{\beta_0}{\beta}\right)}{\sin\left(\frac{\pi\alpha}{2x_0}\right)\sin\left(\frac{\pi}{2x_0}\right)}, \tag{4}$$

and for a 3-gap structure

$$T(\beta) = \frac{\beta}{\beta_0} \frac{\sin\left(\frac{\pi\alpha}{3x_0}\frac{\beta_0}{\beta}\right)\left[\cos\left(\frac{\pi\alpha}{3x_0}\frac{\beta_0}{\beta}\right) - \cos\left(\frac{\pi}{x_0}\frac{\beta_0}{\beta}\right)\right]}{\sin\left(\frac{\pi\alpha}{3x_0}\right)\left[\cos\left(\frac{\pi\alpha}{3x_0}\right) - \cos\left(\frac{\pi}{x_0}\right)\right]}. \tag{5}$$

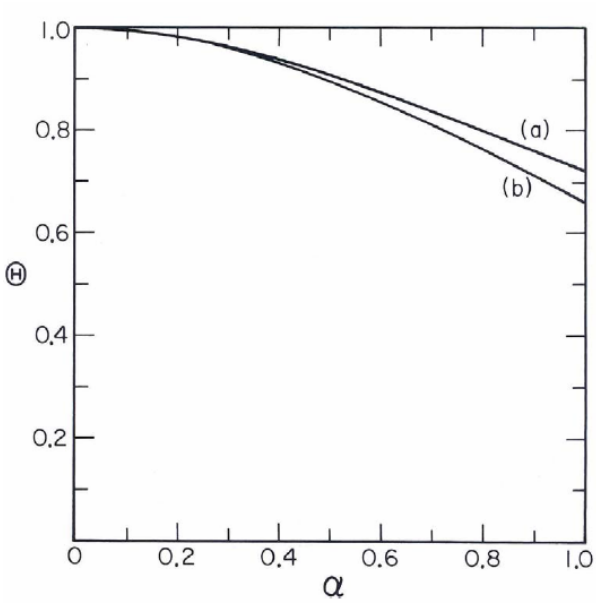

Figure 2: Transit-time factor for 2-gap (a) and 3-gap (b) TEM structures as function of the filling parameter α.

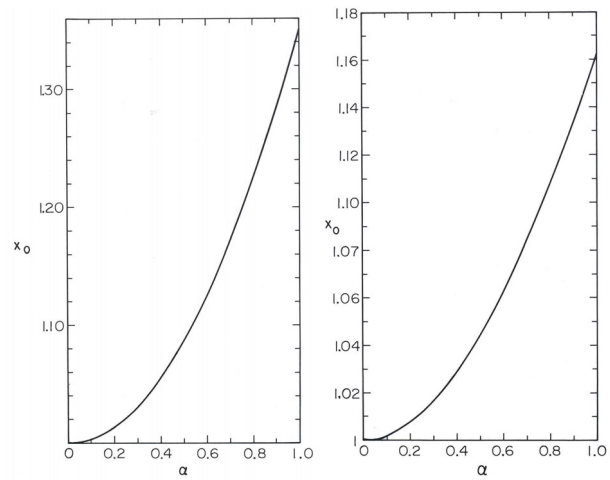

Figure 3: Ratio between actual and geometrical β for 2-gap (left) and 3-gap (right) TEM structures as function of the filling parameter α.

The parameter x_0 is the ratio of the distance between the center of the end gaps and either $\beta_0\lambda/2l$ for a 2-gap structure or $\beta_0\lambda/l$ for a 3-gap structure; it is also the ratio between the actual β_0 of the structure corresponding to the maximum of the velocity acceptance, and the geometrical β of the cavity corresponding to the gap-to-gap distance. As the number of cells increases the parameter x_0 decreases to 1. Graphs for x_0 as a function of the filling parameter α are shown in Fig 3. Note, for example, that, for a 2-gap structure where a typical value of α is 0.5, the distance between the center of the gaps should be about 8% smaller than $\frac{\beta_0\lambda}{2}$.

In TM-class cavities the cell-to-cell coupling is much weaker than it is in TEM cavities, and the perturbation of the end-cell frequency caused by the beam pipe is comparable to that caused by the cell-to-cell coupling. As a consequence, in order to obtain a flat field profile in the π-mode, the end cells are almost identical to center cells. Thus, a good approximation is to assume that the cavity is made of *N* identical cells and the energy gain is

$$\Delta W = q\,V\,\Theta(x)\,\Phi(x)\,, \tag{6}$$

where $x = \beta\lambda/2l$, l being the cell length; V is a reference voltage representing the level of excitation of the cavity; $\Theta(x)$ is the transit-time factor of a single cell and depends on the shape of the field profile, not on its magnitude; $\Phi(x)$ is a phasing factor for a multi-cell structure and depends on the cell length and the amplitude of the field in the cells (which are different in each mode), but does not depend on the field profile as long as it is identical in each cell. In TM structures a sinusoidal field profile is often a good approximation and

$$\Theta(x=\beta\lambda/2l) = \frac{\cos\left(\frac{\pi}{2x}\right)}{1-x^{-2}}\,. \tag{7}$$

Note that for a matched particle we have $\Theta(x=1)=\pi/4$.

A multi-cell cavity can resonate in a number of modes and, because of imperfection in manufacturing and tuning, the accelerating mode will not be a pure π-mode but will also include a linear combination of all the other modes. The phasing factor $\Phi(x)$ represents the interaction between a particle and a mode and can be calculated for all modes. In an *N*-cell cavity operating in mode *M*, the amplitude in cell *j* is

$$V_j^M = \sin\left[\pi M\,\frac{2j-1}{2N}\right], \tag{8}$$

and the phasing factor for mode *M* is

$$\Phi_M(x) = \frac{1}{2}\left\{\frac{\sin\left[\frac{N\pi}{2}\left(\frac{M}{N}-\frac{1}{x}\right)\right]}{\sin\left[\frac{\pi}{2}\left(\frac{M}{N}-\frac{1}{x}\right)\right]} + (-1)^{M+1}\,\frac{\sin\left[\frac{N\pi}{2}\left(\frac{M}{N}+\frac{1}{x}\right)\right]}{\sin\left[\frac{\pi}{2}\left(\frac{M}{N}+\frac{1}{x}\right)\right]}\right\}. \tag{9}$$

Note that for a matched particle (x=1), we have for the π-mode (M=N) $\Phi_N(1)=N$, while for all the non-π-modes we have $\Phi_{M\neq N}(1)=0$. In other words, a particle that is matched to the cavity, as is always the case for $\beta=1$ applications, will interact only with the π-mode component of the accelerating mode but will not interact with all the other components. In intermediate velocity applications, on the other hand, where the β of the particles will not always be matched to the cavity β, the particles may interact with all the mode components of

the accelerating mode depending on how far they are from the matched condition. This is illustrated in Fig. 4 which shows for a 6-cell structure the phasing factor for mode 6 (π=mode), mode 5 (5π/6) and mode 4 (4π/6).

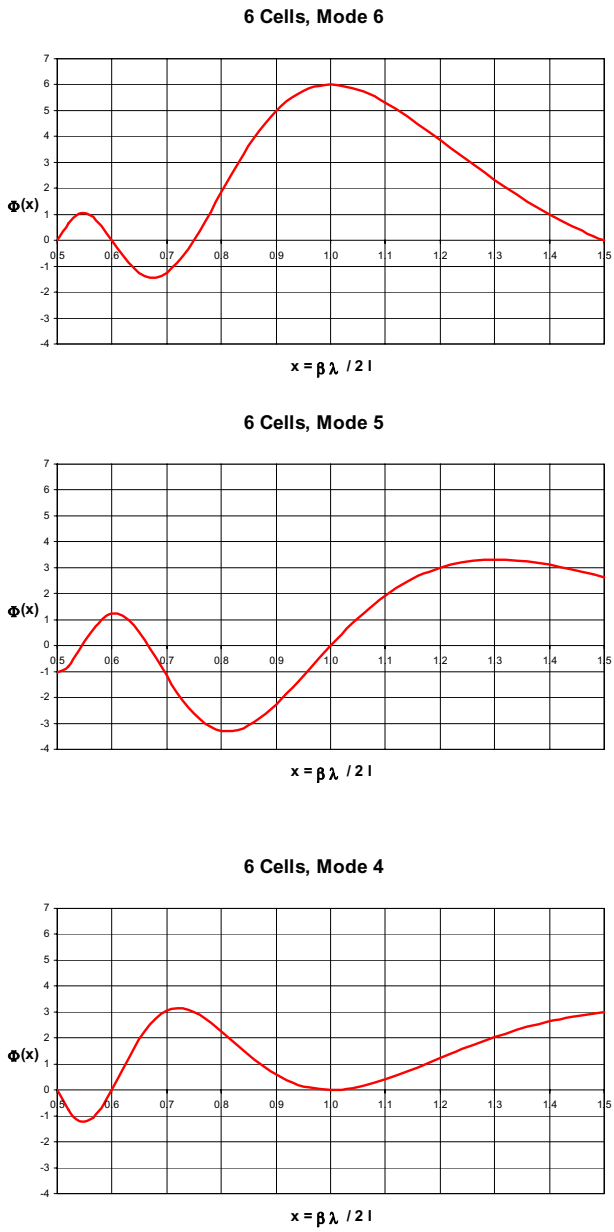

Figure 4: phasing factor for π, 5π/6, and 4π/6 modes in a 6-cell TM cavity as function of particle velocity.

All the previous results are based on the assumption that the velocity of the particle does not change while traversing the cavity. In the low-velocity non-relativistic limit this assumption may not be valid and the energy gain may not be expressed simply by Eq. (2). Even in this case, a simple second-order expression for the energy gain can be found [4]:

$$\Delta W = q\cos\phi\,\Delta W_0\,T(\beta) + \frac{(q\,\Delta W_0)^2}{W}\left[T^{(2)}(\beta) + \sin 2\phi\,T_s^{(2)}(\beta)\right], \tag{10}$$

where W is the kinetic energy, and

$$T^{(2)}(k) = -\frac{k}{4}T(k)\frac{d}{dk}T(k)\,, \qquad k = \omega/\beta c,$$

$$T_s^{(2)}(k) = -\frac{k}{4\pi}\int_0^\infty \frac{T(k+k')\,T(k-k') - T(k)T(k)}{k'^2}\,dk.$$

The new velocity acceptances $T^{(2)}(\beta)$ and $T_s^{(2)}(\beta)$ are not independent functions but are directly related to $T(\beta)$. An example for an actual β=0.1, 3-gap TEM structure is shown in Fig. 5 [4].

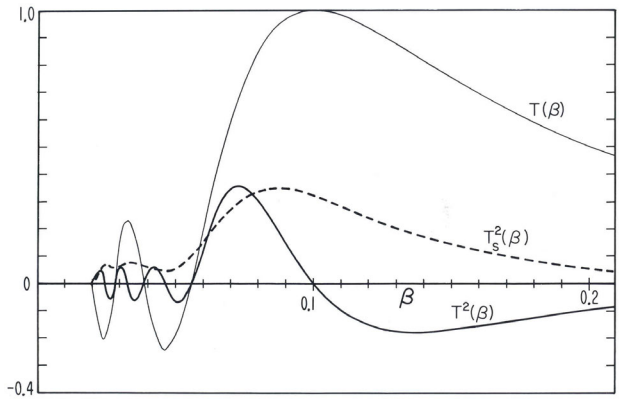

Figure 5: First and second order velocity acceptances for a 3-gap β=0.1 TEM structure.

A SIMPLE MODEL: CAPACITIVELY-LOADED TEM RESONANT LINE

Electrostatic Design of the High-Voltage Region

The high-voltage region of a TEM resonator, whether it is at the end of a λ/4 or in the middle of a λ/2 transmission line, often has a fairly complicated geometry with no simple symmetry. It can, however, be approximated by simple shapes with simple symmetries where the electrostatic problem can be solved, and provide the surface electric fields and loading capacitance with high accuracy. The geometries of interest are

- Cylinder between two planes
- Concentric cylinders
- Sphere between two planes
- Sphere inside a cylinder
- Concentric spheres

These geometries are shown in Fig. 6. In all cases we assume that the center conductor (of characteristic

dimension $2r_1$) is at potential V, while the outer conductor (of characteristic dimension $2r_2$) is at ground potential. Shown in Fig. 7 is $E_p \frac{r_2}{V}$ where E_p is the peak surface electric filed on the center conductor. In essence, it is the ratio of peak surface electric field to accelerating gradient (ignoring the transit time factor Θ defined in the previous section.)

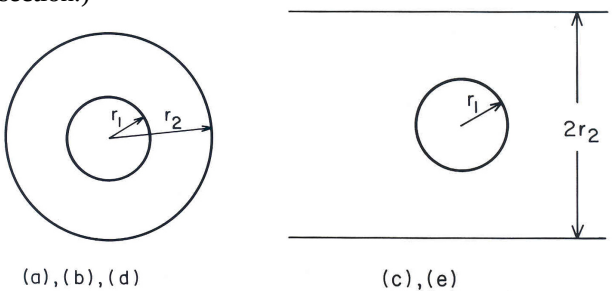

Figure 6: Geometries for several electrostatic configurations: (a) concentric spheres, (b) sphere in cylinder, (c) sphere between 2 planes, (d) concentric cylinders, (e) cylinder between 2 planes.

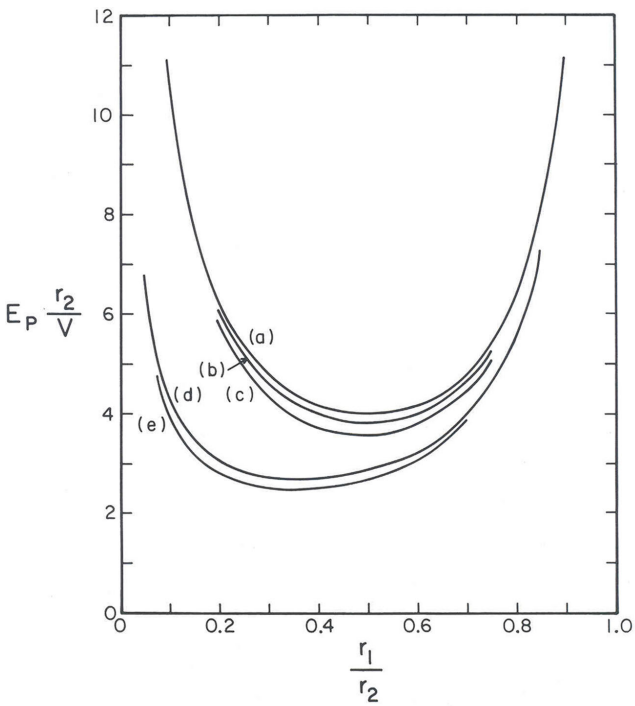

Figure 7: Ratio of peak to accelerating field for the geometries shown in Fig. 6.

Several conclusions can be drawn from Fig. 7. First the surface field is defined mostly by the symmetry of the center conductor. Two-dimensional geometries [(d) and (e)] which are more representative of λ/2 structures have significant lower surface electric fields than three-dimensional geometries [(a), (b), and (c)] which are more typical of the terminations of λ/4 structures. Second, the geometry of the outer conductor has relatively little influence on the surface field. Third, the peak surface field is relatively constant over a wide range of ratio of inner to outer dimensions.

Figure 7 indicates that, for λ/2 structures, the ratio of peak to accelerating field should be slightly less than 3, while, for λ/4 structures, it would be of the order of 4. These numbers should be increased by about 10% due to the transit time factor Θ defined earlier and which has been ignored here. These numbers are probably the best that can be done with a careful design. Lower numbers that are sometimes quoted often result from a particular choice of the accelerating length; on the other hand higher numbers can be obtained for a less than optimal design.

The electrostatic model also produces the capacitance of the termination that is needed to complete the design of the transmission line, especially for λ/4 structures.

Electromagnetic Design of a Transmission Line

Resonant transmission lines are a simple way of generating voltages that can be used to accelerate particles. These are either λ/4 where the line is shorted at one end, and open at the other, or λ/2 where the line is shorted at both ends and the maximum voltage is in the middle. Here we will summarize the basic properties of capacitively-loaded λ/4 transmission lines. A model of such a line is shown in Fig. 8. The results can be easily extended to λ/2 structures by applying factors of 2 at the appropriate places.

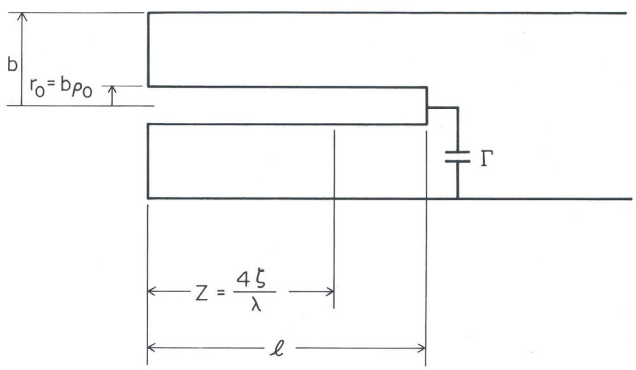

Figure 8: Model of a capacitively-loaded λ/4 coaxial transmission line.

The following notations will be used and the results will be in MKS units:

b : radius of outer conductor

$r(z)$: radius of center conductor

r_0 : radius of center conductor at shorting plate

$\rho = r/b$: normalized radius of center conductor

z : distance from shorting plate

$\zeta = 4z/\lambda$: normalized distance from shorting plate

$\eta = \sqrt{\mu_0/\varepsilon_0} \simeq 377\Omega$: impedance of vacuum

– Capacitance per unit length:

$$C = \frac{2\pi\varepsilon_0}{\ln(b/r_0)} = \frac{2\pi\varepsilon_0}{\ln(1/\rho_0)}. \quad (11)$$

– Inductance per unit length:

$$L = \frac{\mu_0}{2\pi}\ln\left(\frac{b}{r_0}\right) = \frac{\mu_0}{2\pi}\ln\left(\frac{1}{\rho_0}\right). \quad (12)$$

– Current along the center conductor:

$$I = I_0\cos\left(\frac{2\pi}{\lambda}z\right) = I_0\cos\left(\frac{\pi}{2}\zeta\right). \quad (13)$$

–Voltage along the center conductor:

$$V = V_0\sin\left(\frac{2\pi}{\lambda}z\right) = V_0\sin\left(\frac{\pi}{2}\zeta\right). \quad (14)$$

– Transmission line impedance:

$$Z_0 = \frac{V_0}{I_0} = \frac{\eta}{2\pi}\ln\left(\frac{1}{\rho_0}\right). \quad (15)$$

– Loading capacitance:

The transmission line can be shorter than λ/4 and still resonate at the right frequency if it is terminated by the appropriate loading capacitance Γ. The relationship between length z, wavelength λ, and capacitance Γ is given by

$$\Gamma = \lambda\varepsilon_0\frac{\operatorname{cotan}\left(\frac{2\pi}{\lambda}z\right)}{\ln(b/r_0)} = \lambda\varepsilon_0\frac{\operatorname{cotan}\left(\frac{\pi}{2}\zeta\right)}{\ln(1/\rho_0)}. \quad (16)$$

– Gradient/Peak magnetic field:

Neglecting the transit time factor Θ, the energy gain is $2V_p$ over a cavity length (diameter) $2b$. The relationship between the gradient and the peak magnetic field (at the center conductor near the shorting plate) is

$$\frac{E_{\mathrm{acc}}}{B_{\max}} = \frac{V_p}{Bb} = c\,\rho_0\ln\left(\frac{1}{\rho_0}\right)\sin\left(\frac{\pi}{2}\zeta\right) \quad (17)$$

For structures that are not too strongly loaded ($\zeta \simeq 1$) and a center conductor radius close to optimal ($\rho_0 = e^{-1}$) we get $B \approx 9$ mT at 1 MV/m. This value is independent of the frequency and β of the structure.

– Power dissipation (losses on the shorting plate neglected, R_s: surface impedance of material):

$$P = V_p^2\frac{8}{\pi}\frac{R_s}{\eta^2}\frac{\lambda}{b}\frac{1+\rho_0^{-1}}{\ln^2\rho_0}\frac{\zeta+\frac{1}{\pi}\sin\pi\zeta}{\sin^2\frac{\pi}{2}\zeta}. \quad (18)$$

If one assumes that the transverse dimensions scale as β we find

$$P \propto \frac{R_s}{\eta^2}E^2\,\beta\,\lambda^2. \quad (19)$$

– Energy content:

$$U = V_p^2\frac{\pi\varepsilon_0}{8}\lambda\ln^{-1}(1/\rho_0)\frac{\zeta+\frac{1}{\pi}\sin\pi\zeta}{\sin^2\frac{\pi}{2}\zeta}, \quad (20)$$

$$U \propto \varepsilon_0\,E^2\,\beta^2\,\lambda^3.$$

– Geometrical factor:

$$G = QR_s = 2\pi\,\eta\frac{b}{\lambda}\frac{\ln(1/\rho_0)}{1+1/\rho_0}, \quad (21)$$

$$G \propto \eta\,\beta.$$

– Shunt impedance ($4V_p^2/P$):

$$R_{sh} = \frac{\eta^2}{R_s}\frac{32}{\pi}\frac{b}{\lambda}\frac{\ln^2\rho_0}{1+1/\rho_0}\frac{\sin^2\frac{\pi}{2}\zeta}{\zeta+\frac{1}{\pi}\sin\pi\zeta}, \quad (22)$$

$$R_{sh}\,R_s \propto \eta^2\,\beta.$$

– R/Q:

$$\frac{R_{sh}}{Q} = \frac{16}{\pi}\eta\ln(1/\rho_0)\frac{\sin^2\frac{\pi}{2}\zeta}{\zeta+\frac{1}{\pi}\sin\pi\zeta}, \quad (23)$$

$$\frac{R_{sh}}{Q} \propto \eta.$$

Equations (16) to (23) describe the basic electromagnetic properties of constant-radius capacitively-loaded λ/4 transmission lines. These properties can also be summarized in a plot of dimensionless quantities:

– Loading capacitance:

$$\gamma = \frac{\Gamma}{\lambda\varepsilon_0} = \frac{\operatorname{cotan}\frac{\pi}{2}\zeta}{\ln(1/\rho_0)}. \quad (24)$$

– Center conductor voltage ($E_{\mathrm{acc}}/B_{\max}$):

$$v_p = 10^{-8}\frac{V_p}{Bb} = 3\,\rho_0\ln\frac{1}{\rho_0}\sin\frac{\pi}{2}\zeta. \quad (25)$$

– Shunt impedance:

$$r_{sh} = 10^{-6}R_{sh}R_s\frac{\lambda}{b} = \frac{32\times10^{-6}}{\pi}\eta^2\frac{\ln^2\rho_0}{1+1/\rho_0}\frac{\sin^2\frac{\pi}{2}\zeta}{\zeta+\frac{\sin\pi\zeta}{\pi}}. \quad (26)$$

This plot, shown in Fig. 9, presents in a (ζ,ρ) plane the lines of constant γ, v_p, and r_{sh}. In this plot, the solid lines are the lines of constant loading capacitance; they define the length $z = \zeta\lambda/4$ of a coaxial line of constant radius $r_0 = b\rho_0$, terminated by a capacitance Γ, and resonating at a frequency $\omega = 2\pi c/\lambda$. The dashed line then gives the ratio of gradient to peak magnetic field of such a resonator, and the dotted line its shunt impedance.

Since common goals in a structure design are to maximize the shunt impedance and ratio of gradient to magnetic field, it can be clearly seen from Fig. 9 that the

loading capacitance should be as small as possible. This usually is counter to the minimization of the peak surface electric field since that often implies a fairly large high-voltage termination with large radii. Thus the balance between low E_{max} and low B_{max} implies a tradeoff that is application-dependent.

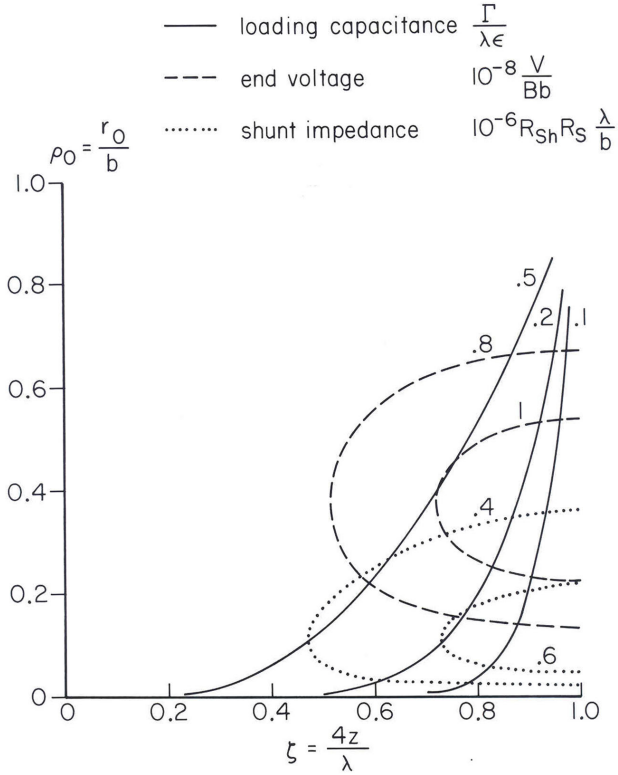

Figure 9: Lines of constant normalized loading capacitance, E_{acc}/B_{max} and shunt impedance for λ/4 constant radius coaxial lines.

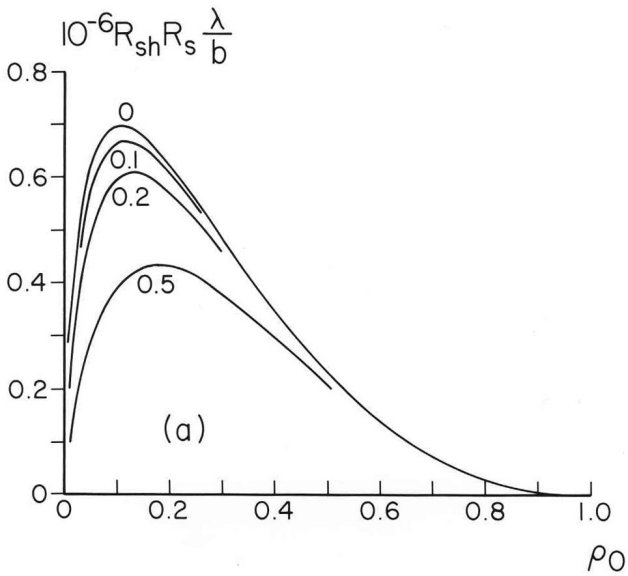

Figure 10: Normalized shunt impedance as function of center conductor radius for various values of the loading capacitance for λ/4 coaxial lines of constant radius.

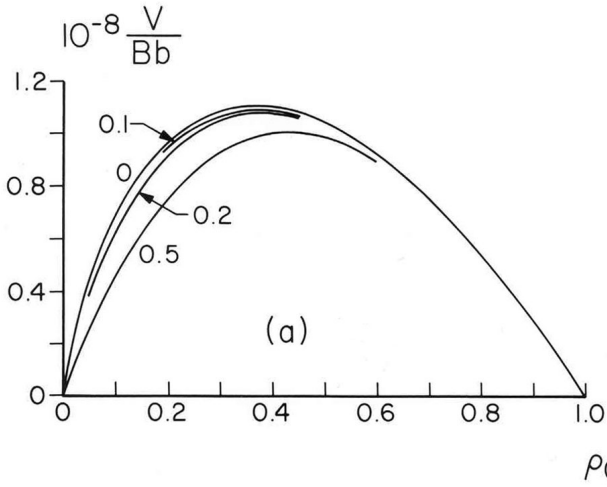

Figure 11: Normalized E_{acc}/B_{max} as function of center conductor radius for various values of the loading capacitance for λ/4 coaxial lines of constant radius.

It can also be seen from Fig. 9 that maximization of the shunt impedance and E_{acc}/B_{max} cannot be achieved simultaneously. The former requires a thin center conductor with $r_0/b \simeq 0.18$ while the latter requires much larger center conductors with $r_0/b \simeq 0.4$. Here also the balance between high R_{sh} and low B_{max} implies a tradeoff that is application-dependent.

Figures 10 and 11 present the same results in a different format. Figure 10 shows the normalized shunt impedance as function of the radius of the center conductor with the loading capacitance as a parameter. Figure 11 is the same for E_{acc}/B_{max}.

All the results presented so far relate to coaxial transmission lines of constant radius; structures of improved properties can be designed with center conductors of variable radius. When the center conductor radius is variable the capacitance and inductance per unit length are position dependent and the voltage and current distribution obey the following equations (see Fig. 12).

$$\begin{aligned}
&\frac{d^2v}{d\zeta^2} - \frac{1}{\rho\ln\rho}\frac{d\rho}{d\zeta}\frac{dv}{d\zeta} + \frac{\pi^2}{4}v = 0,\\
&\frac{d^2i}{d\zeta^2} + \frac{1}{\rho\ln\rho}\frac{d\rho}{d\zeta}\frac{di}{d\zeta} + \frac{\pi^2}{4}i = 0,\\
&\text{where}\quad \rho(z) = \frac{r(z)}{b},\\
&\qquad\quad \zeta = \frac{4z}{\lambda}.
\end{aligned} \tag{27}$$

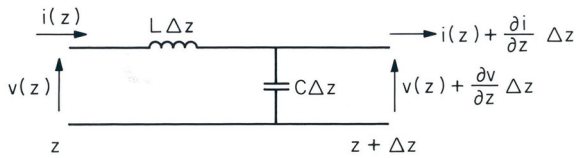

Figure 12: Electrical representation of a section of transmission line with position-dependent parameters.

Such a transmission line can be terminated at any point without changing the voltage and current distribution if the termination reactance is given by

$$\Gamma(z) = -C(z)\frac{i(z)}{di/dz}, \tag{28}$$

Among all the possible shapes for the center conductor, two are of particular interest. The first one is that of constant logarithmic derivative of the capacitance

$$\frac{1}{C}\frac{dC}{dz} = -\frac{1}{d}, \tag{29}$$

corresponding to the center conductor profile

$$r(z) = b\left(\frac{r_0}{b}\right)^{\exp(z/d)} \tag{30}$$

Its interest lies in the fact that it is an almost exact representation of a straight linear taper and that many of its properties can be calculated analytically [6].

Another profile of interest is that of constant surface magnetic field along the center conductor, implying that $r(z) \propto i(z)$. In this case the profile of the center conductor satisfies [6]

$$\frac{d^2\rho}{d\zeta^2} + \frac{1}{\rho \ln \rho}\left(\frac{d\rho}{d\zeta}\right)^2 + \frac{\pi^2}{4}\rho = 0. \tag{31}$$

Its electromagnetic properties can also be calculated and a plot for this profile, similar to Fig. 9 for a constant radius profile, is shown in Fig. 13. In this plot the heavy solid lines are the shapes of the center conductors for several starting radii at the shorting plate. For starting radii $r_0 \sim 0.2 - 0.4\,b$ they are a fair representation of center conductors with a straight section followed by a linear taper. Again, maximizing both a high shunt impedance and E_{acc}/B_{max} implies a small loading capacitance. The

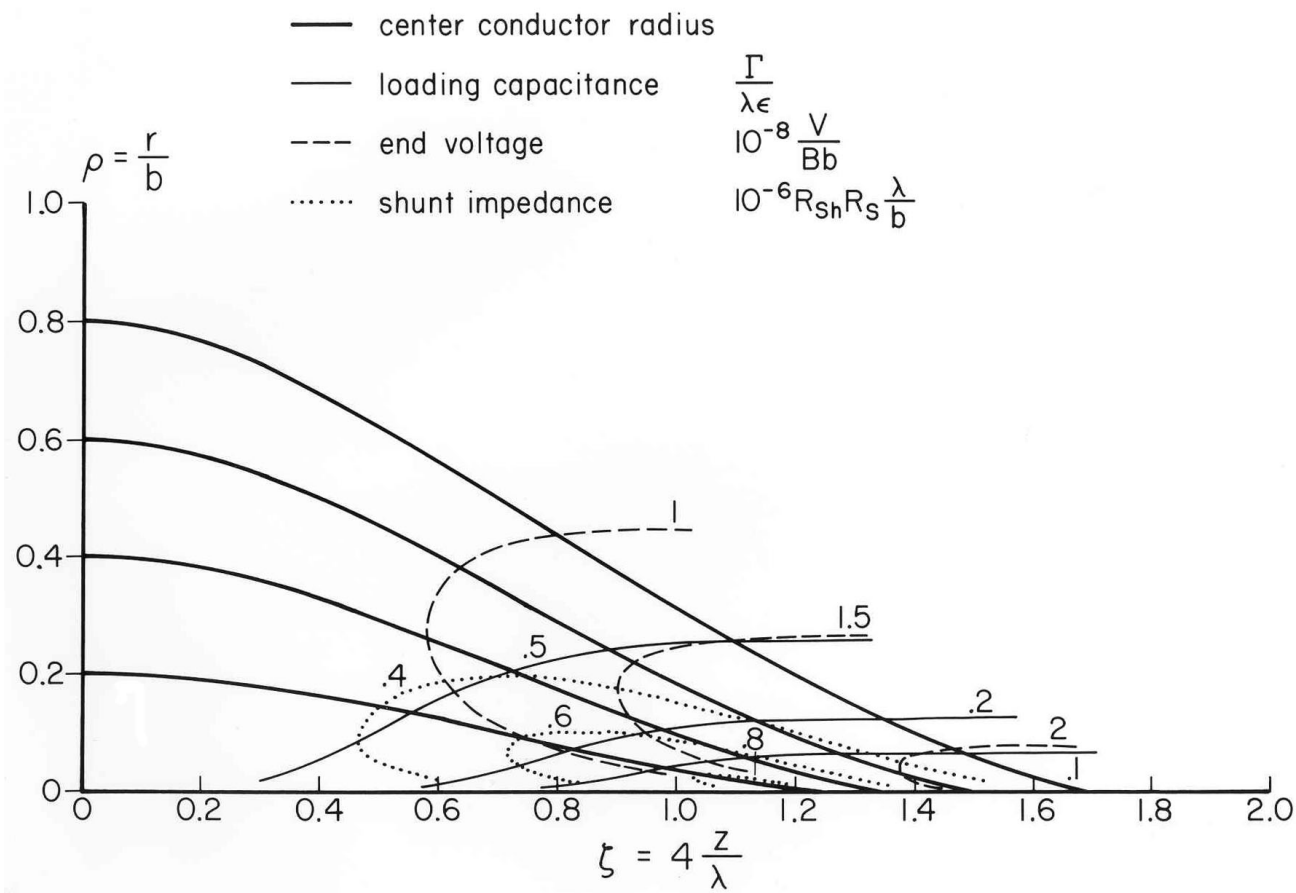

Figure 13: Profile of center conductors and lines of constant normalized loading capacitance, maximum end voltage, and shunt impedance for λ/4 coaxial lines of constant surface magnetic field on the center conductor.

former also implies a starting radius at the shorting plate $r_0/b \simeq 0.18$, while the latter implies a much thicker center conductor.

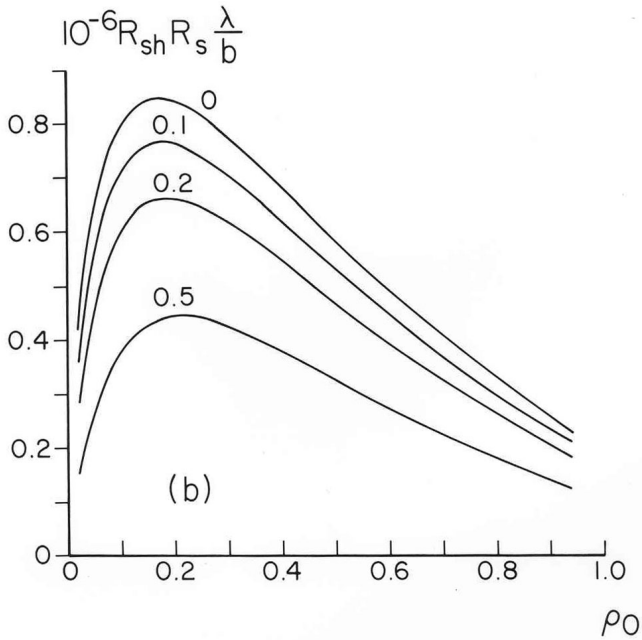

Figure 14: Normalized shunt impedance as function of center conductor radius for various values of the loading capacitance for λ/4 coaxial lines of constant surface magnetic field.

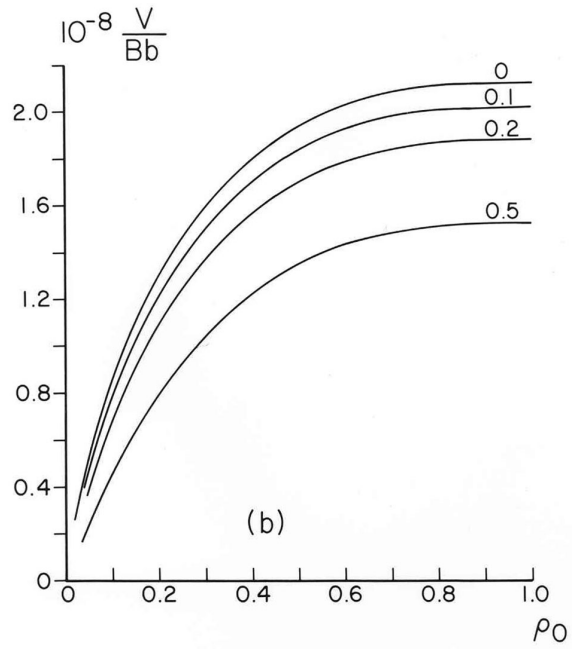

Figure 15: Normalized E_{acc}/B_{max} as function of center conductor radius for various values of the loading capacitance for λ/4 coaxial lines of constant surface magnetic field.

Plots for the profile of constant surface magnetic field, similar to Figs. 10 and 11 for the constant radius profile are shown in Figs. 14 and 15. Comparison between these two sets of plots shows the improvement of the electromagnetic properties provided by profiles of variable cross section.

SUMMARY AND CONCLUSIONS

This paper was intended to be an introduction to issues associated with the design of low- and medium-β superconducting structures. Given the breadth of the subject it had to be selective and superficial. It focused on the electromagnetic properties of TEM-class structures since those of TM-class structures have been addressed much more frequently in the literature [2, 3]. The mechanical design and mechanical properties of low-velocity superconducting structures is another very important part of this field, but has not been addressed. A considerable amount of information on this subject, as well as more in-depth discussions of electromagnetic designs can be found in [6] as well as other contributions to this workshop and other publications [8-20].

For more than 30 years, the development of low- and medium-β cavities has been one of the richest and most imaginative area of srf. Many types of cavities have been developed (helix, spiral, split-ring, quarter-wave, coaxial half-wave, spoke, *etc.*) and the field has been in constant evolution and progress. New geometries have been and are still being developed to address the issues of new applications of the srf technology.

What makes the low and medium beta region so interesting is that the parameter, tradeoff, and option space available to the accelerator structure designer is very large. The geometries are more complex than in the β~1 region and the design process has not been and probably will never be reduced to a few simple rules or recipes. The design of low- and medium-β superconducting structures still offer many opportunities for imagination, originality and common sense.

ACNOWLEDGEMENTS

Many thanks to all the members of the low-β SRF community who, over the years, have provided advice, insight, and information. Special thanks to Jacek Sekutowicz for a thorough review of this paper.

REFERENCES

[1] J. R. Delayen, "Medium-β Superconducting Accelerating Structures," Proc. 10th Workshop on rf Superconductivity, Tsukuba, Japan, 6-11 Sept 2001.

[2] C. Pagani, D. Barni, A. Bosotti, P. Pierini, G. Ciovati, "Design Criteria for Elliptical Cavities," Proc. 10th Workshop on rf Superconductivity, Tsukuba, Japan, 6-11 September 2001.

[3] Sang-ho Kim, "Challenges and the Future of Reduced-β SRF Cavity Design," Proc. LINAC 2002, Gyeongjyu, Korea, 19-23 August 2002.

[4] J. R. Delayen, "Longitudinal Transit Time Factors of Short Independently-Phased Accelerating Structures for Low-Velocity Ions," NIM **A**258 (1987) 15-25.

[5] I. Ben-Zvi, J. M. Brennan, "The Quarter Wave Resonator as a Superconducting Linac Element," NIM **A**212 (1983) 73-79.

[6] J. R. Delayen, "Design of Low-Velocity Superconducting Accelerating Structures Using Quarter-wavelength Resonant Lines," NIM **A**259 (1987) 341-357.

[7] Proceedings of the Workshop on the Advanced Design of Spoke Resonators," Los Alamos 7-8 October 2002, LANL Publication LA-14005-C, compiled by F. L. Krawczyk, This is an excellent source of information on recent work from most of the groups active in the field. http://laacg1.lanl.gov/spokewk/

[8] N. R. Lobanov, D. C. Weisser, E. Zaplatin, "Multi-stub Superconducting RF Resonators for the ANU Heavy Ion Accelerator," these proceedings.

[9] T. Junquera, "Superconducting RF Activities at the IPN Orsay Laboratory," these proceedings.

[10] H. Podlech, H. Deitinghoff, H. Klein, H. Liebermann, U. Ratzinger, A. Suaer, X. Yan, "Status of the Development of a Superconducting 352 MHz CH-Prototype Cavity," these proceedings.

[11] G. Orly, S. Blivet, S. Bousson, F. Chatelet, T. Junquera, J. Lesrel, C. Mielot, A. C. Mueller, H. Saugnac, P. Szott, "Development of SRF Spoke Cavities for Low and Intermediate Energy Ion Linacs," these proceedings.

[12] J-L. Biarotte, S. Blivet, S. Bousson, T. Junquera, G. Olry, H. Saugnac, " Design Study of a 176 MHz SRF Half-wave Resonator for the Spiral-2 Project," these proceedings.

[13] E. Zaplatin, R. Eichhorn, F. M. Esser, B. Laatsch, G. Schug, R. Stassen, R. Toelle, "COSY SC HWR Investigations," these proceedings.

[14] A. Facco, V. Zviagintsev, "A 352 MHz, β=0.31 Superconducting Half-wave Resonator for High-intensity Beams," these proceedings.

[15] V. Zvyaginstev, A. Facco, C. C. Compton, T. L. Grimm, W. Hartung, F. Mari, R. York, "Mechanical Design of a 161 MHz, β=0.61 Superconducting Quarter Wave Resonator with Steering Correction for RIA," these proceedings.

[16] W. Hartung, J. Bierwagen, S. Riecker, J. Colthorp, C. Compton, T. Grimm, S. Hitchcock, F. Mari, L. Saxton, R. C. York, A. Facco, V. Zviaginstev, "Niobium Quarter-wave Resonator Development for the Rare Isotope Accelerator," these proceedings.

[17] G. Devanz, J.-M. Baze, P.-E. Bernaudin, P. Bosland, S. Chel, Y. Morin, F. Nunio, "Quarter-wave Cavities for the Spiral-2 Project," these proceedings.

[18] K. W. Shepard, "Development of Superconducting Intermediate-velocity Cavities for the U. S. RIA Project," these proceedings.

[19] K. W. Shepard, P. N. Ostroumov, J. R. Delayen, "High-Energy Ion Linacs Based on Superconducting Spoke Cavities," Phys. Rev. ST Accel. Beams 6, 080101 (2003).

[20] A. Andreev, G. Bissoffi, A. Pisent, E. Bissiato, M. Comunian, E. Fagotti, T. Shira, "Ladder Resonator: A Novel Superconducting Structure for the Very Low-β Part of High-current Linacs," Phys. Rev. ST Accel. Beams 6, 040101 (2003).